ASCHT 2017
6th Asian Symposium on Computational Heat Transfer and Fluid Flow
10-13 December, 2017
Indian Institute of Technology Madras, Chennai, India

Paper No.265

CHANGE OF FLOW STRUCTURE AND HEAT TRANSFER PERFORMANCE OF PHOTOSENSITIVE MICELLAR SOLUTIONS WITH LIGHT IRRADIATION

Shogo TSUCHIKAWA
Dept. Mech. Eng. and Sci.
Kyoto University
tsuchikawa.shogo.62n@st.kyoto-u.ac.jp

Ikuya SAKANAKA
Dept. Mech. Eng. and Sci.
Kyoto University
sakanaka.ikuya.28r@st.kyoto-u.ac.jp

Takeshi ENYA
Dept. Mech. Eng. and Sci.
Kyoto University
enya.takeshi.68r@st.kyoto-u.ac.jp

Reiko KURIYAMA
Dept. Mech. Eng. and Sci.
Kyoto University
kuriyama@me.kyoto-u.ac.jp

Kazuya TATSUMI
Dept. Mech. Eng. and Sci.
Kyoto University
tatsumi@me.kyoto-u.ac.jp

Kazuyoshi NAKABE
Dept. Mech. Eng. and Sci.
Kyoto University
nakabe@me.kyoto-u.ac.jp

ABSTRACT

This study investigates how the change in flow structure of photosensitive micellar solutions with light irradiation is related to heat transfer performance. Flow visualization and heat transfer measurement were conducted using an aqueous solution of surfactant and counterions (CTAB/NaSal/OMCA) in serpentine channels under $Re^* \sim O(1)$*. The results showed that the decrease in heat transfer rate and pressure drop with the irradiation time are triggered by the decrease of the viscoelasticity of the solution. Flow visualization revealed that the frequency of transition of vortex structure between a single large-scaled vortex and a pair of counter-rotating vortices decreases with the irradiation time, and hence fluid mixture deteriorates. In addition, a pair of vortices are expected to be weakened by decrease of circumferential normal stress, which inhibits the convection of low temperature core to the near-wall area. These two changes in flow structure lead to the deterioration of heat transfer.*

***Keywords*:** viscoelastic fluid flow, heat transfer enhancement, photo-rheological fluid, wormlike micelle

NOMENCLATURE

A_s	Heat transfer area
c_p	Specific heat capacity
De	Dean number
D_h	Hydraulic diameter
f	Fanning friction coefficient
G_0	Plateau modulus
h_m	Mean heat transfer coefficient

k	Thermal conductivity
K	Power-law coefficient
L	Length of channel
$\dot{m}$	Mass flow rate
n	Power-law exponent
Nu_{m}	Mean Nusselt number
ΔP	Pressure drop
Pr	Prandtl number
Re^*	Modified Reynolds number
T	Temperature
U_{m}	Cross-sectional mean velocity
Wi	Weissenberg number
$\dot{\gamma}$	Shear rate
μ	Steady shear viscosity
λ	Relaxation time
ρ	Density
τ	Shear stress

INTRODUCTION

Since electronic devices have been undergoing further integration and minimization of their circuits recently, generation of Joule's heat per unit time and area has been dramatically increasing. In order to remove the heat from the devices, innovative small heat exchangers should be developed. The flows of working fluid in narrow heat transfer channels, however, become laminar because of low Reynolds number flow condition, and thus the mixing and heat transfer performances deteriorate, so far as we use conventional Newtonian fluids like air or water. To tackle such heat transfer problems, the authors' research group has suggested that a photo-rheological fluid (PRF), one of viscoelastic non-Newtonian fluids, should be used as a working fluid to control heat transfer rate with light irradiation [1, 2]. The key concept of this heat transfer control is switching between two states by light irradiation to the fluid according to the demand for heat transfer enhancement; one is the state where heat transfer rate and pressure drop are both high, and the other is the opposite state.

Kawaharada et al. [1] conducted rheological measurement on an aqueous solution of CTAB (cetyl-trimethylammonium bromide), NaSal (sodium salicylate), and OMCA (ortho-methoxy cinnamic acid). The result showed that the viscoelasticity of the solution (hereafter CNO solution) decreased with UV irradiation time, owing to the mitigation of entanglement of wormlike micelles in the solution by photo-isomerization of OMCA. They also made the measurement of heat transfer and pressure drop using the same CNO solution, and showed that both heat transfer coefficient and pressure drop decreased with UV irradiation time, triggered by the decrease of viscoelasticity. The obtained heat transfer results must be attributed to flow structure which is closely linked with the micelle structures, but the flow structure has not been clearly investigated yet.

The purpose of the present study is to investigate how the change of the flow structure of CNO solution by UV irradiation is related to the change in heat transfer performance. The authors conducted heat transfer and pressure drop measurement using a heated copper serpentine channel and flow visualization using a transparent channel of the same shape and size. We referred to the previous numerical study for steady flow of polymeric fluids [3, 4] to compare them with both results and discuss closely.

WORKING FLUIDS

Wormlike Micellar Solution

The micelle structure varies with surfactant concentration, ionic strength and temperature and becomes wormlike in certain conditions [5]. Wormlike micelles form entangled networks in high concentration, and consequently wormlike micellar solutions exhibit distinctive non-Newtonian rheological behaviors. The viscosities of most of such solutions decrease as shear rate $\dot{\gamma}$ increases, which is known as shear-thinning phenomenon, and they generally obey the power law ($\mu(\dot{\gamma}) = K\dot{\gamma}^{n-1}$) in a particular range of $\dot{\gamma}$ [6]. K and n are referred to as power-law coefficient and power-law exponent, respectively. Furthermore, most wormlike micellar solutions have viscoelasticity because entangled networks of micelles add elasticity to viscosity. The elastic stress of the solutions decreases with time due to reptation motion and break-up of micelles. The time scale of the decrease of the elastic stress is referred to as relaxation time. Most wormlike micellar solutions obey Maxwell model, where the viscoelastic characteristics of the solutions are represented by only two properties; relaxation time (λ) and plateau modulus (G_0) [5]. Wormlike micellar solutions seem to flow differently from Newtonian fluids and consequently enhance heat transfer because of these non-Newtonian behaviors.

In this study an aqueous solution of CTAB/NaSal/OMCA (CNO solution) was used as a kind of wormlike micellar solutions. CTAB is a cationic surfactant molecule. NaSal and OMCA are both counterions of CTAB. Counterions stabilize the micelle structure by weakening the repulsion of hydrophilic groups of surfactant molecules. The concentrations of CATB, NaSal and OMCA were 1.0wt%, 0.20wt% and 0.20wt%, respectively. 20mM NaOH was added to the solution in order to increase the solubility of OMCA.

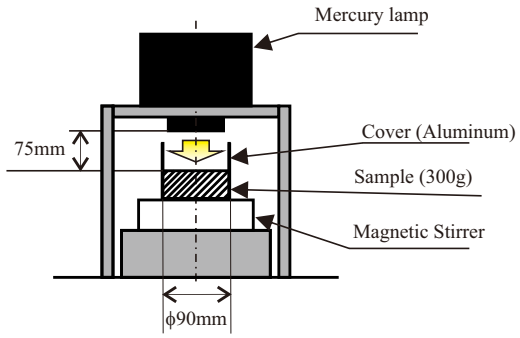

FIGURE 1. LIGHT IRRADIATION APPARATUS.

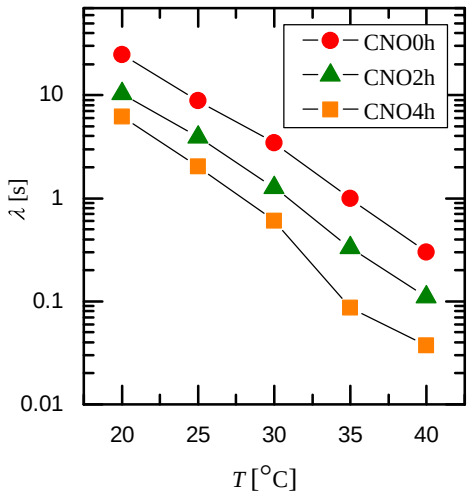

FIGURE 2. TEMPERATURE DEPENDENCE OF RELAXATION TIME.

Rheological Change by Light Irradiation

OMCA is a photo-sensitive molecule which has two geometrical isomers. Exposed to UV, *trans*-OMCA isomerizes to *cis*-OMCA. Although this isomerization is reversible, it is apparently irreversible from *trans*-OMCA to *cis*-OMCA because *trans*-OMCA is more likely to be activated by UV than *cis*-OMCA is. Since *trans*-OMCA develops wormlike micelles better than *cis*-OMCA, the viscoelasticity of CNO solution decreases with UV irradiation owing to the gradual isomerization of OMCA.

In the present study CNO solutions were prepared with *trans*-OMCA (without *cis*-OMCA) initially and exposed to UV using the apparatus shown in Fig. 1. Each 300g CNO solution was exposed to UV emitted from a 100W Mercury lamp (Olympus, U-LH100HFAPO) for 0, 2 or 4 hours, which is referred to as CNO0h, CNO2h or CNO4h, respectively. During light irradiation, the samples were stirred by a magnetic stirrer at 150rpm with a $14\times\phi 40$mm cross-head stir bar.

TABLE 1. RHEOLOGICAL PROPERTIES OF CNO SOLUTIONS AT 20 °C.

Fluid Name	K	n	λ [s]	G_0 [Pa]
CNO0h	4.38	0.004	24.2	3.42
CNO2h	3.62	0.033	9.04	2.95
CNO4h	2.61	0.033	4.90	2.47

Measurements of steady shear viscosity and dynamic viscoelasticity were conducted for the prepared samples using a rheometer (Anton Paar, MCR301). The measured rheological properties at 20°C are listed in Tab. 1. The measured values of steady viscosity was fully fitted with the power law within the range of $10\text{s}^{-1} \leq \dot{\gamma} \leq 100\text{s}^{-1}$, as is reported in the previous work [1]. In Tab. 1 K, λ and G_0 decreased with light irradiation time, which means viscoelastic properties decreased [5]. As shown in Fig. 2, λ of each CNO solution exponentially decreases with temperature and becomes one tenth as the temperature rises by 10K, although a different tendency was observed in CNO4h case at higher than 30°C.

EXPERIMENTAL METHOD

Test Channel

The schematic of the serpentine channel used in this study is shown in Fig. 3. The channel has the square cross-section of 5mm, and hydraulic diameter D_h is 5mm. The serpentine section consists of semicircles of inner radius R_i =5mm and outer radius R_o =10mm alternating from side to side and repeating ten times periodically. We call the semicircle unit which is Nth from upstream simply Nth unit.

The flows of micellar solutions in this channel were evaluated by modified Reynolds number Re^* and Weissenberg number Wi, which are defined by

$$Re^* = \frac{\rho U_\text{m}^{2-n} D_\text{h}^n}{8^{n-1} K (B + A/n)^n} \tag{1}$$

$$Wi = \lambda \dot{\gamma}_\text{m} = \frac{4U_\text{m}\lambda}{D_\text{h}}, \tag{2}$$

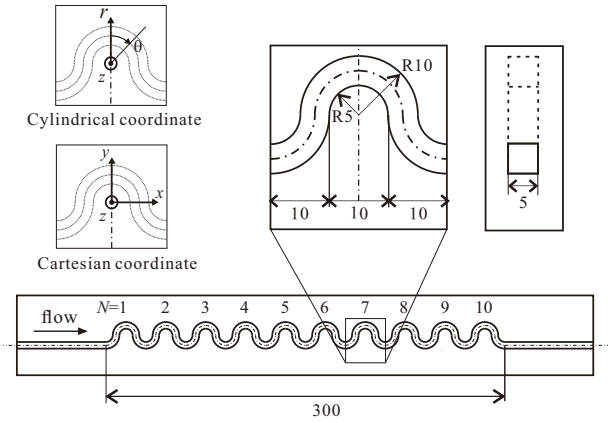

FIGURE 3. DIAGRAM OF TEST CHANNEL (UNIT: MILLIMETER).

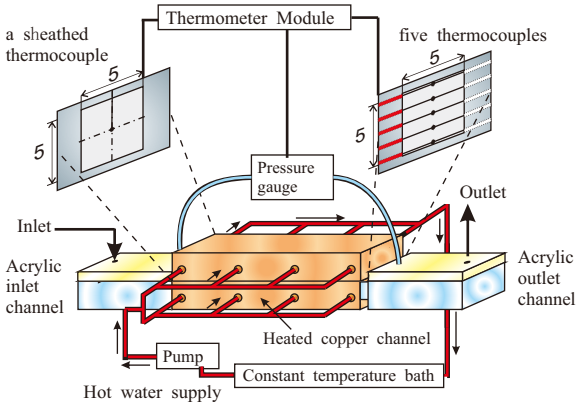

FIGURE 4. DIAGRAM OF HEAT TRANSFER AND PRESSURE DROP MEASUREMENT APPARATUS.

TABLE 2. CONDITIONS OF HEAT TRANSFER AND PRESSURE DROP MEASUREMENT.

Fluid	Re^*	De	Wi	Pr
CNO0h	1.8-11	0.7-5.4	45-170	800-1900
CNO2h	2.2-10	1.2-5.5	31- 71	600-1300
CNO4h	1.7-12	0.9-6.2	8.4- 52	650-1400

respectively. ρ, U_m, and $\dot{\gamma}_\mathrm{m}$ are density of fluid, cross-sectional mean velocity, and representative shear rate, respectively. A and B are geometric parameters, whose values are 0.2121 and 0.6766, respectively, in a square channel. The density of pure water was used as ρ because the solutes of CNO solutions are sufficiently dilute. Re^* was defined so as to satisfy the relation that Fanning friction coefficient f is equal to $16/Re^*$ in a laminar flow in an arbitrary cross-sectional straight channel in isothermal condition [7]. Weissenberg number Wi was used to evaluate the effect of elastic stress.

In addition, Dean number De is defined by

$$De = \frac{\rho U_\mathrm{m} D_\mathrm{h}}{\mu}\sqrt{\frac{D_\mathrm{h}}{R_\mathrm{o}+R_\mathrm{i}}}, \tag{3}$$

so as to evaluate the effect of centrifugal force in the curved channel. The value of Dean number was less than 10 in this study, as will be mentioned below. In such low De conditions, Dean instability does not occur for the flow of Newtonian fluid. It was experimetally confirmed that there was no Dean instability by running Newtonian fluid (an aqueous solution of 64.4wt% sucrose) through our test channel in the same range of Dean number condition.

Method of Heat Transfer and Pressure Drop Measurement

The schematic of the experimental apparatus used in this measurement is shown in Fig. 4. The shape and size of the channel are same as those shown in Fig. 3. This experiment was conducted under a constant wall temperature condition by circulating hot water, whose temperature was kept at 40°C, through the copper wall. Pressure drop in the test section ΔP was measured using two pressure gauges (Keyence; AP-C30) connected to the upstream and downstream of the test channel, and evaluated by Fanning friction coefficient $f = D_\mathrm{h}\Delta P/(2\rho U_\mathrm{m}^2 L)$, where the total channel length L was 471mm. Wall temperature T_w was measured using four K-type thermocouples attached on the outer surface of the copper channel. Spatial average of T_w varied within 0.5°C with time. The inlet bulk temperature $T_\mathrm{b,i}$ and the outlet bulk temperature $T_\mathrm{b,o}$ were measured using thermocouples inserted in the channel as shown in Fig. 4. We calculated $T_\mathrm{b,o}$ by weighting the theoretical velocity profile on the measured outlet temperature profile. The theoretical velocity profile was obtained as

$$\frac{u(y,z)}{U_\mathrm{m}} = \frac{2.1157}{2}\cdot\frac{3n+1}{n+1}\left[1-\left(\frac{y}{2.5}\right)^{(1.2n+1)/n}\right] \cdot\left[1-\left(\frac{z}{2.5}\right)^{(1.2n+1)/n}\right], \tag{4}$$

with regard to the fully-developed flow of power-law fluid in square-cross-sectional channel [8, 9]. Considering the equation of energy on the heat transfer target wall where heat

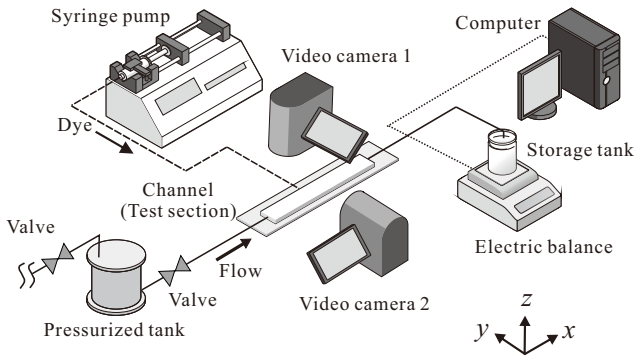

FIGURE 5. DIAGRAM OF FLOW VISUALIZATION APPARATUS.

transfer coefficient is constant at h_m, mean Nusselt number Nu_m is obtained as

$$Nu_m = \frac{h_m D_h}{k} = \frac{\dot{m} c_p D_h}{k A_s} \times \ln \frac{T_w - T_{b,i}}{T_w - T_{b,o}}, \qquad (5)$$

where k, A_s, $\dot{m}$, and c_p are thermal conductivity of fluid, heat transfer area, mass flow rate and specific heat capacity of fluid, respectively.

Heat transfer and pressure drop measurements were conducted under the conditions shown in Tab. 2, where Pr is Prandtl number. A series of measurements were conducted under room temperature (20°C), and logarithmic mean temperature of fluid (T_m) varied from 25°C to 35°C depending on the conditions. We substituted the values of c_p and k by those of pure water and used the thermal and rheological properties at T_m in each measurement.

Method of Flow Visualization

The test channel of this experiment was made of polycarbonate and has the shape and size shown in Fig. 3. The diagram of flow visualization apparatus is shown in Fig. 5. A 0.8mm-outer-diameter SUS tube was inserted horizontally into the test channel between 7th unit and 8th unit so as to supply dye for visualization. One end of the SUS tube was capped and the other was connected to a syringe pump by way of the polyethylene tube. The SUS tube has a tiny lateral hole at the center of cross-section of the channel, through which dye was ejected by the syringe pump. We put two video cameras and recorded flow patterns at the 9th unit from two different directions; top view from positive z-direction (video camera 1) and side view from negative y-direction (video camera 2). A series of experiments were conducted under $Re^* \sim 2$, and detailed conditions are shown in Tab. 3.

TABLE 3. CONDITIONS OF FLOW VISUALIZATION.

Fluid	Re^*	De	Wi	Dye flow rate [μL/min]
CNO0h	2.1	2.8	677	250
CNO2h	2.3	1.6	259	180
CNO4h	1.8	1.3	104	190

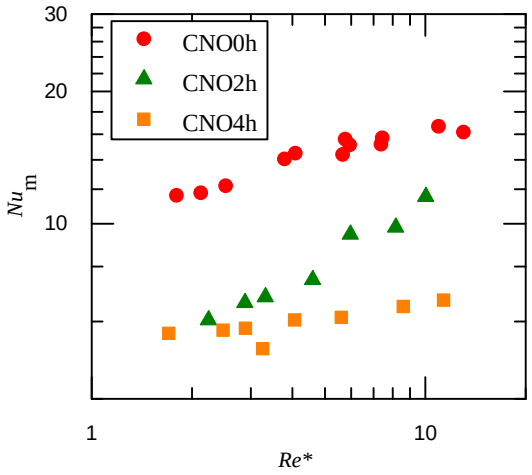

FIGURE 6. RELATION BETWEEN MODIFIED REYNOLDS NUMBER AND MEAN NUSSELT NUMBER WITH CNO SOLUTIONS.

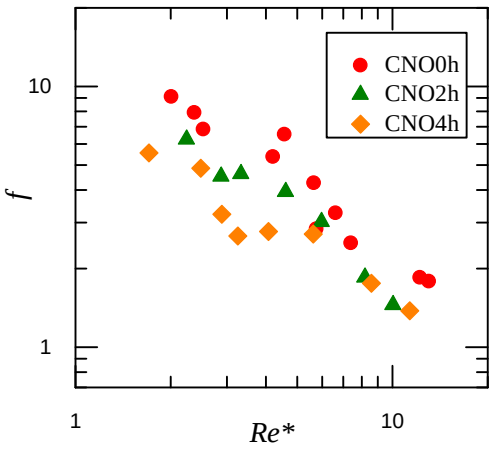

FIGURE 7. RELATION BETWEEN MODIFIED REYNOLDS NUMBER AND FANNING FRICTION COEFFICIENT WITH CNO SOLUTIONS.

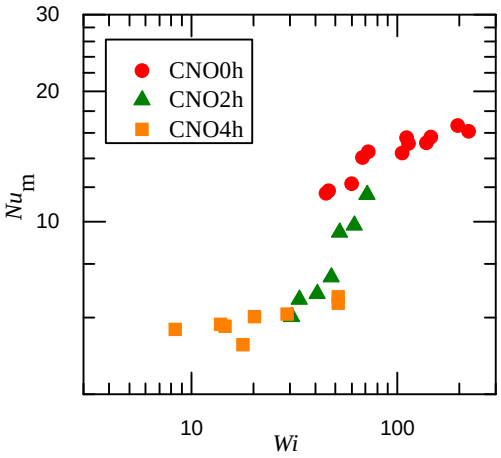

FIGURE 8. RELATION BETWEEN WEISSENBERG NUMBER AND MEAN NUSSELT NUMBER WITH CNO SOLUTIONS.

RESULTS AND DISCUSSTIONS

Results of Heat Transfer and Pressure Drop Measurement

Mean Nusselt number Nu_m and Fanning friction coefficient f of CNO solutions are plotted in terms of modified Reynolds number Re^* in Figs. 6 and 7, respectively. The symbol of each solution in these figures corresponds to that in Fig. 2. In Fig. 6 Nu_m decreases with light irradiation over the whole range of Re^*. In CNO4h case Nu_m is smaller than half the value of CNO0h case at each Re^*. As shown in Fig. 7, f gradually decreases with light irradiation, showing a certain dispersion of the obtained data due to technical limitation in the pressure measurement. The increase in Nu_m and f in a serpentine channel with the rise in K and λ is consistent with previous study dealing with polymeric solutions [3].

The results shown in Fig. 6 are also plotted in terms of Weissenberg number Wi in Fig. 8, where Re^* is not fixed at a constant value. The figure shows that Nu_m increases with Wi. Further, the plots of every light irradiation time case exist almost on a single curve. Tatsumi et al. [3] reported that a good agreement was observed in the relation between Wi and Nu_m among three polymeric fluids with different concentration, and Nu_m started to increase at $Wi \sim 30$. These aspects are consistent with the present results. These two studies suggest that Nu_m has stronger dependence on Wi than on Re^*. In other words, the change of heat transfer characteristics by light irradiation time relies more on viscoelastic behavior than on viscous behavior. The flow structures which lead to heat transfer characteristics will be discussed in the following subsections.

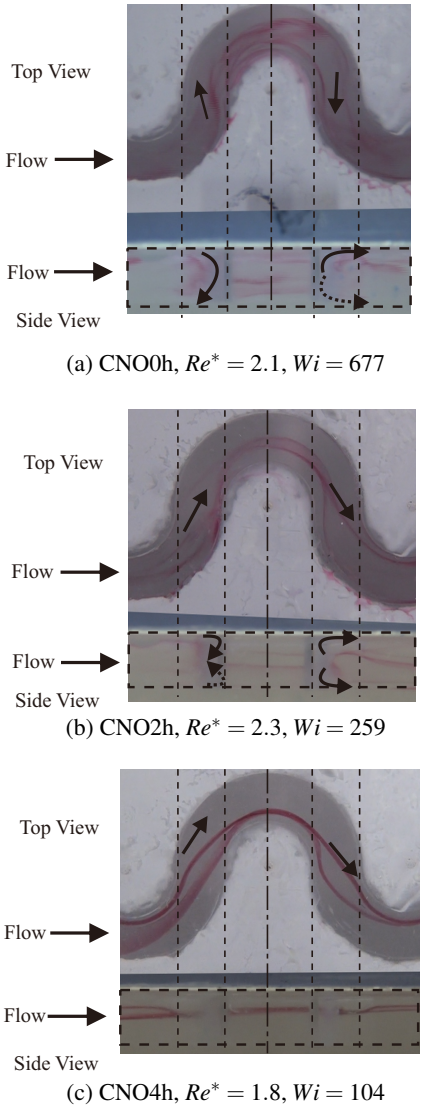

(a) CNO0h, $Re^* = 2.1$, $Wi = 677$

(b) CNO2h, $Re^* = 2.3$, $Wi = 259$

(c) CNO4h, $Re^* = 1.8$, $Wi = 104$

FIGURE 9. FLOW PATTERNS VISUALIZED IN A SERPENTINE CHANNEL.

Results of Flow Visualization

Flows of CNO solutions in a serpentine channel were visualized by dye streakline under the conditions listed in Tab. 3. The rough flow pattern in the movies was unsteady in both CNO0h and CNO2h cases, and it was more perturbed in CNO0h case. In contrast, the flow pattern in CNO4h case was almost steady although slight fluctuation of the streakline was observed. Further, the fast flow near the side wall was more frequently observed in CNO0h case than in CNO2h and CNO4h cases.

Typical flow patterns visualized in the movies are shown by instantaneous snapshots of movies in Fig. 9. The

upper part of each figure shows the top view recorded by video camera 1 and the bottom part shows the side view by video camera 2. The solid arrows in Fig. 9 represent the flow directions which are obvious from the streaklines, and the dotted arrows represent the expected flow directions. In the top view movie of each condition, the flows orientated from outer wall to outer wall (Fig. 9 (a)) and those orientated from inner wall to inner wall (Fig. 9 (b)(c)) were observed near the inflection points of the channel, or connecting parts of neighboring semi-circles. Note that the flow orientations in CNO0h and CNO2h cases alternated intensively with time in contrast to CNO4h case, where it was steady from inner wall to inner wall.

Moreover, two types of vortices were observed in the side view movies; one is a single large-scaled vortex and the other is a pair of counter-rotating vortices, as shown in the side view of Fig. 9. A single vortex rotates in a large circle over the whole cross-section. A pair of vortices rotate from the center of cross-section to the top/bottom walls. As will be detailed in the next subsection, the previous numerical work for steady flow of viscoelastic fluid showed that a pair of vortices are generated in cross-sections of a serpentine channel [3]. Although a pair of vortices were not always observed clearly, when either vortex was observed, we expected that the other vortex rotating in a counter direction existed considering the result of the previous computation. Such expected vortices are drawn with the dotted arrows in Fig. 9 (a)(b). In Fig. 9 a single vortex was observed in the left-hand inflection point of (a), and pairs of vortices were observed in the right-hand of (a) and in the both-hand of (b).Both two types of vortices were observed alternately in CNO0h and CNO2h cases. In contrast, secondary flows were not distinct in CNO4h case. Emergence of a single vortex was more frequent in CNO0h case than in CNO2h case.

Relation between Flow Structure and Heat Transfer Characteristics

The present experimental results shown in the former subsections are summarized as follows. As the viscoelasticity of CNO solutions decreases with light irradiation time, flow unsteadiness and longitudinal type of a single vortex gradually decreases, and the heat transfer performance deteriorates. In this case, the location of the area where the flow velocity shows the maximum value in the cross-section is not near the channel wall but near the center of the channel and the pressure drop decreases. To further discuss the relationship between the flow structure and heat transfer characteristics, we will compare our experimental results with those of numerical computation reported by Tatsumi et al. [3].

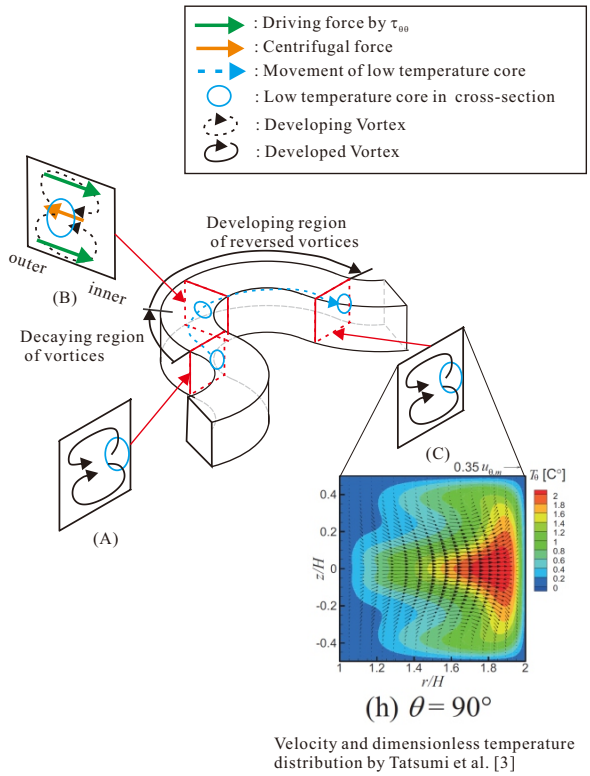

FIGURE 10. SCHEMATIC OF THE FLOW PATTERNS WITH A PAIR OF VORTICES OBTAINED IN PREVIOUS COMPUTATION.

Their computation was made for flow in a serpentine channel of same geometry as the present study under the condition of $Re = 0.63$, $Wi = 205$ and $De = 0.13$. From their results, we have drawn the schematic of the vortices structure generated in the channel as shown in Fig.10. This figure shows secondary flow structure, driving forces of secondary flow, and location of the low temperature region on cross-sections which are located at the inflection points (A, C) and at the midpoint of the curve (B). In addition, the figure involves the result of their computation corresponding to the cross-section(C), which shows the distribution of velocity vectors and dimensionless temperature $T_\theta = (T - T_\mathrm{w})/(T_\mathrm{b,o} - T_\mathrm{w})$ in the cross-section. T_θ becomes large when fluid temperature is low and becomes 0 when it is same as T_w. A pair of counter-rotating vortices is generated in the cross-section (B) by radial forces produced in the near wall region of top and bottom walls owing to the normal stress differences and circumferential stress $\tau_{\theta\theta}$. The vortices develop by these forces along the curvature and show maximum strength at the inflection point. Downstream of the inflection point, the vortices decay and their rotating

direction becomes opposite due to change of the curvature direction. By the pair of vortices, low temperature core region is convected from the inner wall area to the outer wall area as it flows downstream through the semi-circle region. Heat transfer is, therefore, enhanced at the inner sidewall at upstream inflection point and at the outer sidewall at downstream inflection point.

The present experimental results showed that heat transfer performance of CNO solutions decreases as the viscoelasticity decreases by light irradiation. The cause is considered as follows referring to the numerical results mentioned above. Decrease in viscoelasticity leads to decrease of the driving force generated by $\tau_{\theta\theta}$. This decreases the strength of the pair of vortices. Consequently, low temperature fluids region is located at the center of the cross-section, and thus, the heat transfer at the sidewalls decreases.

Considering the present results of flow visualization, further discussion can be given as follows. While a pair of counter-rotating vortices were observed in both the flow visualization and the previous computation, a single large-scaled vortex was observed only in the flow visualization. The reason seemed that the computation was conducted for steady flow, and namely the term depending on time was eliminated. Therefore, the term may enhance the instability of flow and generate a single vortex. Such flow instability may increase as Wi increases, considering the results of the flow visualization. According to the present results, heat transfer performance increases with increase in the frequency of a single vortex. The transition from a pair of vortices to a single vortex can increase the mixture of fluid and enhance heat transfer. Namely, the strength of a pair of vortices and the mixture of fluid by transition of vortex structure seem the cause of the change of heat transfer performance by light irradiation to CNO solutions. Since the quantitative values for these aspects were not obtained in this study, extra quantitative experiments like PIV measurement should be conducted henceforth.

CONCLUSION

Heat transfer and pressure drop measurement and flow visualization in serpentine channels were conducted using a kind of photosensitive micellar solutions. The results obtained in the present study are summarized as follows.

- As time of light irradiation to the solution increases, the relaxation time, a representative of viscoelastic properties, of the solution was decreased, and heat transfer rate and pressure drop were decreased in the range where Reynolds number is 1 to 20.
- Two types of vortical flow patterns were visualized; one is a single large-scaled vortex and the other is a pair of counter-rotating vortices. As the viscoelasticity of the solution decreased with light irradiation, emergence of a single vortex became infrequent, and thus mixture of fluid decreased. In addition, the strength of a pair of vortices is expected to be weakened owing to decrease of the circumferential normal stress. These changes in flow structure can be main causes of the decrease in heat transfer performance.

REFERENCES

[1] Kawaharada, K., Fujii, T., Enya, T., Tatsumi, K., and Nakabe, K., "Light-turning of Heat Transfer Performance for Low Reynolds Number Flow of Micellar Solution", *Proc 1st Int. Pac. Rim Thermal Eng. Conf.*, PRTEC-14717,(2016).

[2] Enya, T., Kuriyama, R., Tatsumi, K., and Nakabe, K., "Heat Transfer Control by Light Irradiation to Low Reynolds Number Flows Using Photosensitive Micellar Solution", *Proc 4th Int. Forum on Heat Transfer*, IFHT2016-1986,(2016).

[3] Tatsumi, K., Nagasaka, W., Matsuo, T., and Nakabe, K., "A Numerical and Experimental Study on Flow and Heat Transfer Characteristics of Viscoelastic Fluid Flow in a Serpentine Channel", *Proc 15th Int. Heat Transfer Conf.*, IHTC15-9615,(2015). See also http://ihtcdigitallibrary.com/conferences/ihtc15,1fc8f93d0f741cd0,644f0217677da4bc.html.

[4] Nakayama, K., Tatsumi, K., and Nakabe, K., "Numerical Study on Unsteady Flow and Heat Transfer Characteristics of Viscoelastic Fluids in Serpentine Channels", *Proc 1st Int. Pac. Rim Thermal Eng. Conf.*, PRTEC-14859, (2016).

[5] Ezrahi, S., Tuval, E., and Aserin, A., "Properties, Main Applications and Perspectives of Worm Micelles", *Adv. Colloid Interface Sci.*, Vol. 128-130 (2006), pp. 77-102.

[6] Miller, E., and Rothstein, J. P., "Transient Evolution of Shear-banding Wormlike Micellar Solutions", *J. Non-New. Fluid Mech.*, Vol. 143 (2007), pp. 22-37.

[7] Kozicki, W., Chi. H., and Tiu, C., "Non-Newtonian Flow in Ducts of Arbitrary Cross-Sectional Shape", *Chem. Eng. Sci.*, Vol. 21 (1966), pp. 665-679.

[8] Wiginton, C. L., and Dalton, C., "Incompressible Laminar Entrance Flow in a Circular Sector Duct", *J. Appl. Mech.*, Vol. 37(1970), pp. 196-203, Academic Press.

[9] Shah, R. K. and London, A. L., "Laminar Flow Forced Convection in Ducts", (1978), pp. 196-203, Academic Press.